

1 Perego R. ^a, Guandalini R. ^b, Fumagalli L. ^a, Aghib F.S. ^c, De Biase L. ^a, Bonomi T. ^a

2

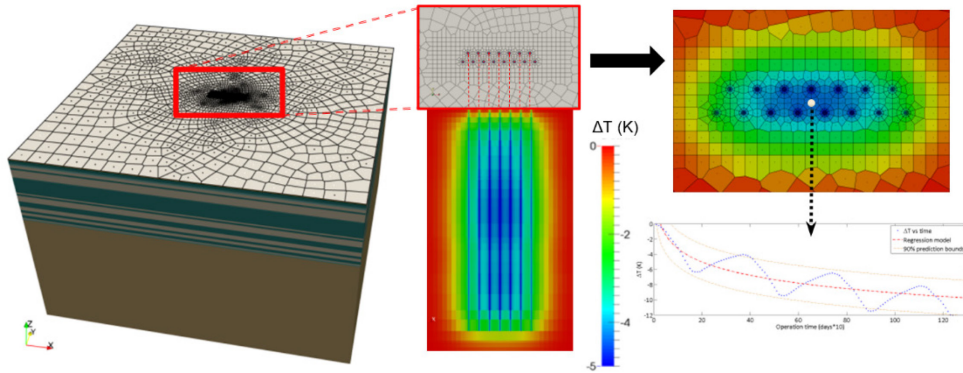
3 Sustainability evaluation of a medium scale GSHP system in layered alluvial setting using 4 3D modeling suite

5

6 ^a Department of Earth and Environmental Sciences, University of Milano-Bicocca, Piazza della Scienza 1, Milano, Italy

7 ^b RSE Spa (Research on Energy System), Department of Environment and Sustainable Development, Via Rubattino 54, Milano, Italy

8 ^c CNR IDPA – National Research Council of Italy. Department of Dynamics of Environmental Processes



9

10 **Abstract**

11 In this study the performances and the environmental effects of a medium scale GSHP system located in
12 Alessandria (Italy) and installed in an highly heterogeneous alluvial setting are considered. The system was
13 monitored over a year and data showed a progressive loss of efficiency. Simulation results show that the
14 analyzed GSHP system has an inadequate design even for a short/medium period operation in an extremely
15 heterogeneous alluvial background as the considered one. A strong probe interference phenomenon was
16 observed, due to the particular layout of the probe field and due to the high energy request for building
17 conditioning. The efficiency loss is also amplified by the presence of an alluvial framework with low thermal
18 properties. The use of a homogeneous subsurface with mean thermal properties reduces thermal imbalance
19 issues by 25% while the improvement of probe distance by 55% produces a reduction of thermal imbalance
20 by 45%. In this case study the homogeneous subsurface assumption leads to excessive simplification of the
21 observed strong heterogeneity and it underrates thermal impact on the soil, especially in layers with poor
22 thermal properties.

23 **Keywords:** Ground source heat pump (GSHP) system, ground heterogeneity, probe interference, alluvial
24 setting, TOUGH2

25

26

27

Nomenclature

$\Delta T=(T_0-T_i)$	temperature variation	(K)
T_0	initial temperature	(K)
T_i	temperature computed at i -th time step	(K)
F	flux of superscript component	kg m ² /s or W/m ²
n	orthogonal vector entering the interface	-
q	mass or heat sink/source term	kg/s m ³ or J/s m ³
M	mass accumulation term	kg
m	cell number	-
V	volume	m ³
k	matrix of absolute permeability	-
k_r	relative permeability	-
$\nabla P= P_0-P_{cap}$	P is the reference pressure and P_{cap} the capillary pressure	Pa
g	component of gravity vector in θ direction of flow, measured along vertical direction	m/s ²
θ	Angle between connection and the vertical	°
D	molecular diffusion coefficient	m ² /s
X	mass fraction	
$F_{m,n}$	average value of the normal incoming flux component on the portion of surface A_{mn} , between volumes V_n and V_m	
$d_{n,m}$	distance between nodal points n and m	m
g	acceleration of gravity vector	m/s ²
J	discretized form of diffusive flux	mol/m ² s
S	phase saturation	
t	time	s
R	residual term at $i+1 - th$ time step	-

Greek letters

λ	thermal conductivity	W/m K
Γ	closed surface for integrals	m ²
μ	viscosity	kg /m s
ρ	density	kg/m ³
τ	tortuosity factor	-
ϕ	porosity	%
δ	Factor that includes a porous medium dependent factor and a coefficient that depends on phase saturation	-

Subscripts and superscripts

β	phase number
k	component number
n, m	nodal point number
i	number of temporal step

Abbreviations

GSHP	Ground Source Heat Probe
GWHP	Groundwater Heat Probe

GRT	Ground Response Test
CCS	Carbon Capture & Storage
CAES	Compressed Air Energy Storage
ILS	Infinite-Line (heat) Source
FLS	Finite-Line (heat) Source
L	probe characteristic length

28

29 **1. Introduction**

30

31 Geothermal energy can play a valuable role in reducing the amount of greenhouse gas emissions caused by
32 the combustion of fossil fuels. A very interesting aspect of this type of energy, based on the heat radiated by
33 the sun and the heat flux from the interior of the Earth to the surface, is its suitability for energy production, for
34 buildings heating/cooling and for hot water production. A number of different technologies can be considered
35 for its exploitation. This paper focuses on low enthalpy systems, a very advantageous type of geothermal
36 technology that deals with low temperature differences and does not require geothermal reservoirs with high
37 porosity, permeable rocks or anomalous temperature gradients as it happens for medium and high enthalpy
38 systems. The application of this type of technology in several European countries has been very profitable and
39 has seen a significant growth in the last 14 years [1] [2], resulting in emissions and costs saving [3]. In other
40 countries, such as Italy, this technology has recently began to develop in a relevant way with applications that
41 involve large energy demands, buildings and volumes (i.e. Lombardy Region headquarters with 6 MW of
42 thermal power produced by groundwater heat pumps (GWHP) and INPS offices in Genoa with 400 kW
43 produced by ground source heat pumps (GSHP). Low enthalpy geothermal systems require large initial
44 investments but are subject to low maintenance costs and are more efficient than usual heating/cooling
45 systems [4]. Without considering the cost/benefit topic, it is very important to correctly define the layout and
46 the characteristics of these systems at a commercial and neighborhood scale rather than at single user scale
47 in order to reduce errors related to plant design [5] [6] and holding down costs that affect the return on
48 investments period [7]. More specifically, the installation of closed-loop GSHP systems must take into account
49 a correct identification of thermal ground properties [8], the possible presence and influence of groundwater
50 flow [9], the knowledge of climate conditions [10] (required for horizontal systems but negligible for vertical
51 systems) and the design parameters of the GSHP system itself [11] [12]. Strictly environmental issues caused
52 by closed-loop GSHP systems could be identified in potential groundwater pollution caused by a spillage of
53 the antifreeze solution used as thermo vector fluid [13] or in the overexploitation of the thermal field. Thermal
54 issues are easily resolved for small GSHP systems, where thermal energy demand is usually limited to few
55 kW·h and thermal interference caused by adjacent probes is absent, but they become more serious when

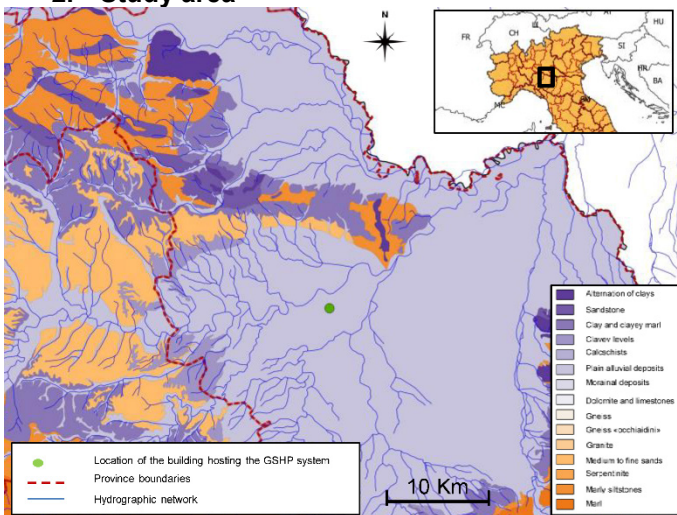
56 GSHP are used to satisfy ever greater energetic demands and to condition environment of increasing size
57 [14].

58 Energetic and environmental issues related to the previously mentioned aspects have been characterized in
59 literature with both analytical models [15] [16] [17] [18] and numerical ones. Numerical methods, which could
60 be powerful tools in order to previously identify and characterize potential environmental and efficiency issues
61 (using both Finite Elements Method as well as Finite Difference Methods) have been more frequently used in
62 closed-loop GSHP systems simulations to assess thermal performances of vertical energy piles [19] or to
63 predict heat exchange rates for a ground-source heat probe system [20]. In Cui et al. [21] numerical methods
64 have been used for the simulation of ground-coupled heat probe applications in alternative operation modes
65 over a short time. Hecht Mendez et al. [22] used numerical methods to optimize energy extraction of a BHE
66 field when groundwater flow occurs while Kim et al. [23] simulated temperature changes in a BHE with fluid
67 circulating through U-tubes. However, literature and the cited documents did not properly consider 3D-
68 temperature field in the ground and rarely the influence of major factors such as thermal imbalance, ground
69 heterogeneity or probe thermal interference is investigated using fully 3D numerical models. The environmental
70 standpoint is often neglected, preferring to strictly focus on energetic issues. It is often omitted the possibility
71 of obtaining environmentally sustainable systems without compromising an optimal energetic efficiency. In
72 heating periods unsustainable GSHP system could perform excessive heat extraction leading to soil freezing
73 (that leads to pressure increase) and frost heave which could damage structures, foundations or plant roots.
74 In cooling periods, excessive heat injection would also overheat the ground, causing soil dilatation and drying.
75 The recovery of the thermal field carried out on a defective or inadequate GSHP system allows to increase the
76 environmental sustainability of the system also acting on the energetic efficiency, reinstating the system at
77 optimal performance levels.

78 Furthermore, most of the scientific papers related to closed-loop GSHP systems deal with slightly
79 heterogeneous subsurface or they simulate ideal case studies with probes inserted in homogeneous grounds
80 neglecting the possibility to properly characterize thermally critical layers. This could lead to an unexpected
81 performance loss due to a localized alteration of the thermal field. Closed-loop GSHP systems in highly
82 heterogeneous alluvial stratigraphy with poor thermal properties that commonly affects densely populated
83 areas aren't often discussed. In particular the Po Plain, one of the most productive and energetically
84 demanding areas of Italy, is affected by alluvial framework and the efficiency of large closed-loop GSHP
85 systems installed herein can be limited by poor ground thermal properties.

86 This paper reports a study that is part of a M.Sc. thesis [24] carried out at RSE Spa in the frame of the project
87 “Studies and assessments of rational use of electrical energy” funded by the Italian Ministry of Economic
88 Development. The work engages the previously explained environmental and operating aspects related to a
89 medium scale vertical GSHP installation by means of a fully 3D numerical approach based on an Integrated
90 Finite Difference Method (IFDM) for fluid dynamic simulations coupled with a detailed geophysical model. At
91 first, the study analyses the critical behavior of a closed-loop GSHP system installed in Alessandria (Italy) and
92 described in Guandalini et al. [25] for which 1 year of experimental data have been measured, showing a
93 progressive loss of efficiency. The real case study is assessed through the originally developed GeoSIAM
94 modeling system in order to properly understand the causes of these specific efficiency issues, characterizing
95 critical layers and assessing the main causes of thermal imbalance in highly heterogeneous subsurfaces (such
96 as Po Plain alluvials). The study then investigates the effect of different parameters on vertical, horizontal and
97 3D ΔT distributions. Different design suggestions were also hypothesized with the aim of recovering the
98 environmental conditions, concurrently allowing a partial recovery of the plant efficiency. Lastly short-term
99 simulations for each scenario were analyzed and data regression was performed in order to estimate average
100 medium-term ΔT values and temperature stabilization times for every simulation scenario.


101 2. Study area



102 The analyzed GSHP system is located within a building placed in the town of Alessandria (Italy) (Fig. 1). The
103 geological setting of the city is constituted of fluvial and lacustrine Holocene deposits, related partly to
104 postglacial floods and partly to recent fluvial deposits [26]. The geomorphology of this area is characterized by
105 the presence of Bormida and Tanaro rivers. Regional geological sections illustrate that the uppermost 100
106 meters of sediments are constituted of clay and gravel, occasionally interspersed with sandy lenses, while the
107 lower 50 meters are mainly composed of sandstones. A more accurate stratigraphic characterization of the
108

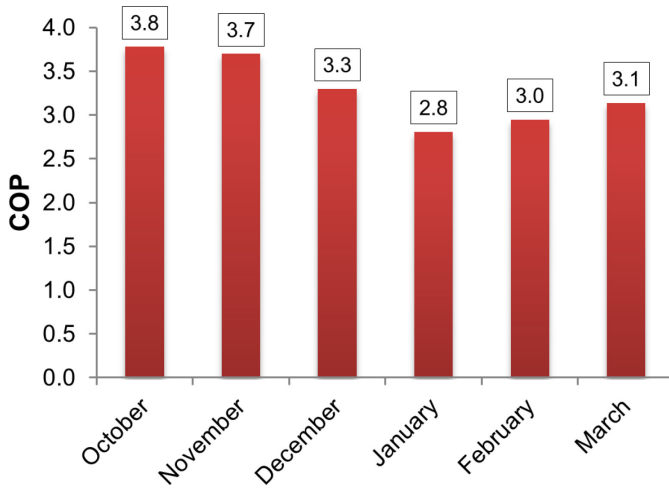
109 subsurface for the investigated GSHP system has been carried out using 109 well logs derived from boreholes
 110 located within Alessandria district and near the building site. Due to these data, it has been possible to create
 111 an “average” reference stratigraphy (Fig. 2). Well logs data were provided by the Italian Geological Service
 112 and by Geographic Information System of ARPA Piemonte, while physical and thermal properties of the
 113 lithological layers have been extrapolated from Tinti [27] and integrated with VDI 4640 blatt 1 [28] because no
 114 experimental data were available. A single GRT test is not reliable for large scale systems and alone cannot
 115 guarantee the real efficiency of the system. The use of a heterogeneous model arises from the need to properly
 116 characterize the critical layers and the stratigraphy described in Fig. 2 seems to be a reasonable representation
 117 of the strong heterogeneity observed in the subsurface of the study area. However, some studies similarly
 118 show that, in some cases, homogeneous models would tend to provide valid results even in multi-layer
 119 backgrounds [29]. Important climatic elements of this area are related to freezing phenomena and absence of
 120 thaw during winter so the system is located within a heating-dominated district [30]. There is also the presence
 121 of a phreatic aquifer at a depth of approximately 8-9 m, having an estimated hydraulic gradient of 0.0005 [26]
 122 and an average groundwater velocity of few m/y. The influence of the aquifer flow on the installed GSHP
 123 system has been therefore hypothesized to be negligible for the purposes of this study due to its very low
 124 hydraulic gradient and the small thickness of the aquifer compared to aquicludes thickness.

Layer	Description	Thickness (m)	Bottom depth (m.b.g.l.)	Effective porosity (%)	Dry thermal conductivity (W/m K)	Wet thermal conductivity (W/m K)	Specific heat (J/kgK)	Material density (kg/m ³)
1	Soil	1.5	-1.5	41	0.5	1.7	494	2025
2	Clay	4.3	-5.8	6	0.5	1.7	1000	1600
3	Sand	2.8	-8.6	40.3	0.4	2.4	912	1920
4	Peat	0.3	-8.9	90	0.4	1.8	1800	770
5	Gravel	4.7	-13.6	24	0.4	1.8	1267	1500
6	Clay	2.5	-16.1	6	0.5	1.7	1000	1600
7	Gravel	13	-29.1	24	0.4	1.8	1267	1500
8	Sand	0.5	-30.6	40.3	0.4	2.4	1167	1920
9	Clay	25	-55.6	6	0.5	1.7	1000	1500
10	Gravel	2.5	-58.1	24	0.4	1.8	1267	1600
11	Clay	3	-61.1	6	0.5	1.7	1000	1500
12	Gravel	10	-71.1	24	0.4	1.8	1267	1600
13	Clay	9	-80.1	6	0.5	1.7	1000	1500
14	Gravel	7	-87.1	24	0.4	1.8	1267	1600
15	Clay	4	-91.1	6	0.5	1.7	1000	1500
16	Gravel	5	-96.1	24	0.4	1.8	1267	1600
17	Clay	5	-101.1	6	0.5	1.7	1000	1500
18	Gravel	2	-103.1	24	0.4	1.8	1267	1600
19	Sand	2	-105.1	40.3	0.4	2.4	912	1920
20	Sandstone	5	-110.1	22.2	2.3	2.3	898	2450



126
127

3. Geothermal heat probe system: description and performances



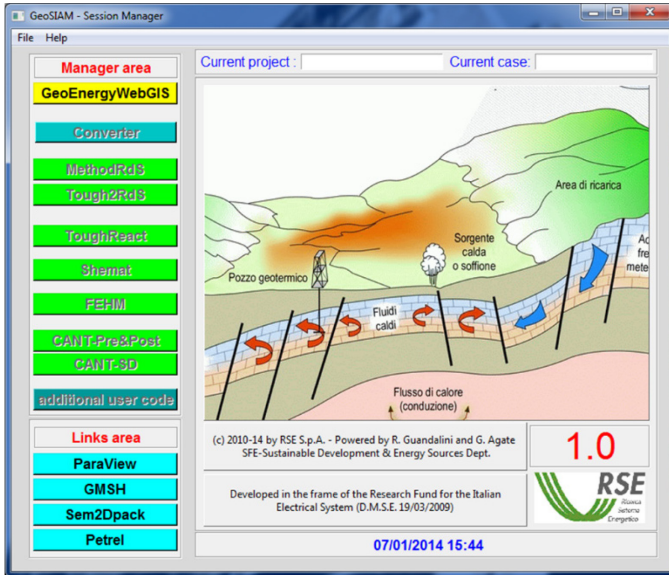
128

129 The analyzed GSHP layout includes 15 vertical ground heat probes used to heat twelve apartments of 80 m².
130 Each probe is 100 m long and is constituted of a 1U-type vertical closed-loop providing a nominal thermal
131 power of 67 kW to the building. The thermo-vector fluid is water mixed with a small percentage of ethylene
132 glycol, used in order to avoid freezing conditions during the winter. The 15 probes are arranged in two
133 staggered rows, the northern of which includes 7 probes, while the southern one includes the remaining 8,
134 with an average distance between adjacent probes of 4.5 m. A summary of main features related to both GSHP
135 system and building is reported in Table 1. Measured data regarding the analyzed GSHP system range from
136 October 2009 to March 2010 as summarized in Table 2, with an average heat extraction rate from the ground
137 of 50 kW and a total of 121817 kW·h (4.385E+11 J) removed. Data show that fluid outlet temperature reaches
138 critical low values probably due to a corresponding decrease of ground temperature and this effect becomes
139 stronger when heat demand is higher and air temperature becomes lower, such as in January and February.
140 As a consequence GSHP system efficiency slowly decreases in time. This is confirmed by the COP index trend
141 (Fig. 3), defined as the ratio between the thermal energy Q provided by the heating system and the electrical
142 energy W required by the heat probe (Q/W) that varies from a value of 3.8 in October to a value of 2.8 in
143 January. Moreover, data show that the mean daily temperature of water coming from the geothermal field has
144 generally been lower than air temperature. From an energetic standpoint the Primary Energy Ratio (PER),
145 defined as the ratio between the produced thermal energy and the primary energy (derived from fossil fuels)
146 used to produce the consumed electrical energy [31] has a value of 1.27 (evaluated considering an electric
147 efficiency η_e of 46% [32]). It is believed that the energetic efficiency of the system could be improved because
148 it derives from low operating temperatures during time, so the first step of the study was to assess the causes
149 of this phenomenon reproducing it by a properly generated numerical model.

150

151
152

4. GeoSIAM



153

154 The numerical simulation of the GSHP system aimed at investigating the loss of performances detected from
155 the measured data requires the creation of a 3D-model able to account for both the ground heterogeneities
156 and the probe structure. This 3D model must have a sufficiently accurate spatial detail and physical property
157 description in order to reproduce the behavior of thermal field during operating and stand-by periods. GeoSIAM
158 (Integrated System for GeoModeling Analyses) [33] is a fully integrated software suite (Fig. 4) which modules
159 are devoted to the numerical simulation of the fluid dynamic, geochemical and geo-mechanical aspects of
160 problems related to the characterization of geological sites for CO₂ storage (CCS), compressed air energy
161 storage (CAES) and exploitation of geothermal fields. The system includes pre and post-processing modules,
162 simulation modules, auxiliary tools and a captivating user-friendly graphic interface that supports the user in
163 the optimization of potential design and simulation scenarios. The spatial detail of generated models varies
164 from the centimeter scale of the probe structures to the meter scale of surrounding region. The modeling suite
165 is composed of a GMSH module for the basic 2D mesh generation, MethodRdS modeler for generation of the
166 3D numerical simulation model, fluid dynamic simulator Tough2RdS and the graphic visualizer ParaView [34]
167 for result analysis.

168 The physical model has been generated by MethodRdS with the aim of describing in the most accurate way
169 the heterogeneity of the geological domain as summarized in (Fig. 2). The modeler generates the final 3D
170 simulation model coupling a static geological 3D representation of the materials with an unstructured spatial
171 mesh based on the Voronoi tessellation technique [35]. The resulting polyhedral cells have optimized

172 dimensions for a detailed description both of the probe structure and the surrounding region. Furthermore, the
 173 ability of the modeler to create cells with a different number of faces (up to 22) and with different shapes allows
 174 to represent geological structures in a very realistic way. This feature is particularly useful in high-enthalpy
 175 geothermal modeling where thermal reservoir formations are often represented by regional structures
 176 generated by calderas and by anticlines/synclines. Probe structures have very small dimensions compared to
 177 the domain scale, so a grid refinement is required along with a proper definition of the probe itself. Grid
 178 refinement is automatically realized by the modeler starting from the initial Voronoi node distribution coming
 179 from the geological model and refining it adding a number of supplemental nodes in the region where the probe
 180 structures must be included. These complex structure must be connected with the surrounding mesh with cell
 181 rings progressively increasing in dimension, in order to avoid numerical instabilities and to assure the isotropy
 182 of heat exchange.

183 The transient simulation of the fluid and heat fluxes during the operating period is carried out by the GeoSIAM
 184 Tough2RdS simulator by selecting a proper state module able to evaluate the physical phenomena occurring
 185 in a low enthalpy scenario. Tough2RdS has been developed in RSE starting from the well-known native
 186 TOUGH2 code [35], modified in order to adapt it to a larger number of users and adding different features
 187 especially oriented to CCS and to advanced geothermal applications, making it more user-friendly over the
 188 entire model creation process.

189 In the IFDM approach, the flux of fluids through porous media is governed by both physical and empirical
 190 relations. Mass balances, momentum and heat are represented by partial differential equations that describe
 191 the variation fluid phase saturation (ρ_β), temperature (T) and pressure (P) as functions of time and space into
 192 the subsurface domain. Referring to the mesh generated as previously explained, it is possible to calculate
 193 mass balance and energy balance for the fluid component k in m^{th} cell, having a volume V_m , using the following
 194 equation:

$$195 \quad \int_{\Gamma_n} F^{(k)} \cdot nd\Gamma_n + \int_{V_n} q^{(k)} dV_n = \frac{d}{dt} \int_{V_n} M^{(k)} dV_n \quad (1)$$

196 The first integral term represents the orthogonal (normal) flux, the second one represents the source term and
 197 the third represents the net mass change in time for the V_m volume of m^{th} cell.

199 The individual flux components are given by Darcy's law:

$$200 \quad F_\beta^{(k)} = -k \frac{k_{r\beta}}{\mu_\beta} \rho_\beta X_\beta^{(k)} (\nabla P_\beta - \rho_\beta \mathbf{g} \cos \theta) - \delta_{\beta g} D_{va} \rho_\beta \nabla X_\beta^{(k)} \quad (2)$$

201 Mass balances of water and salt, along with heat balance, are set up and solved by Tough2RdS using the

202 Newton-Raphson iteration method. In order to obtain a numerical solution, the previously described equations
 203 must be appropriately discretized by a series of non-linear algebraic equations coupled for every cells (or node)
 204 and they can be solved through appropriate linearization techniques, using iterative solvers. Therefore, every
 205 term of Equation 2 can be defined as a mass accumulation term:

$$206 \int_{V_n} M dv = V_n M_n \quad (3)$$

207 where M_m represents the average value of M into V_m volume. The total flux term crossing the interface is given
 208 by:

$$209 \int_{\Gamma_n} F^{(k)} \cdot n d\Gamma_n = \sum_m A_{mn} F_{mn}^{(k)} \quad (4)$$

210 The discretized form of flux can be described using the average values within V_n and V_m volumes, while the
 211 rate term included into Darcy's relation can be approximated by :

$$212 F_{\beta, nm} = -k_{nm} \left[\frac{k_{r\beta} \rho_\beta}{\mu_\beta} \right]_{nm} \left[\frac{P_{\beta, n} - P_{\beta, m}}{d_{nm}} - \rho_{\beta, nm} \mathbf{g}_{nm} \right] \quad (5)$$

213 The amounts expressed by the previous equations are calculated at the interface, so it is necessary to define
 214 the flux parameters and the fluid state at the interface. In order to calculate these parameters, many averaging
 215 algorithms are available, such as linear interpolation, harmonic weighting and upstream weighting, The choice
 216 of the weighting methodology has a great influence on results therefore it is appropriate to perform a
 217 preliminary evaluation of the accuracy of the calculated flux through monitored values. The discretized form of
 218 diffusive flux related to X of k component between elements n and m is given by:

$$219 J_{\beta, nm}^k = -(\Phi S_\phi \tau_\beta)_{nm} (D_\beta^k)_{nm} \rho_{\beta, nm} \frac{X_{\beta, n}^k - X_{\beta, m}^k}{d_{nm}} \quad (6)$$

220 In Equation 6 harmonic weighting is used to evaluate the $\Phi S_\phi \tau_\beta$ term at the interface, while D and ρ are
 221 averaged on block n and m volumes. A set of first order differential equations is obtained by performing
 222 appropriate substitutions in the initial balance equation, :

$$223 \frac{dM_n^k}{dt} = \frac{1}{V_n} \sum_m A_{nm} F_{nm}^k + q_n^k \quad (7)$$

224 Time is discretized by first order finite differences. Flux and source terms are evaluated at time:

$$225 t^{i+1} = t^i + \Delta t \quad (8)$$

226 ensuring the required numerical stability to obtain an efficient computation of multi-phase fluid. This approach
 227 is entirely implicit, because fluxes are expressed as a function of unknown thermodynamic parameters at t^{i+1}
 228 time. Fully implicit IFDM form of the previous system becomes:

$$229 \quad M_m^{(k)i+1} - M_m^{(k)i} - \frac{\Delta t^i}{V_m} \left\{ \sum_n A_{mn} F_{mn}^{(k)i+1} + V_m q_m^{(k)i+1} \right\} = R_m^{(k)i+1} \cong 0 \quad (9)$$

230 where

$$231 \quad \Delta t^i = t^{i+1} - t^i \quad (10)$$

232 is the incremental variable in time at i^{th} step, R is the residual term at $i+1^{th}$ step that has to be minimum after a
 233 predetermined number of iterations, otherwise temporal step is automatically reduced. Total flux is then given
 234 by:

$$235 \quad F_{\beta,mn}^{(k)} = k_{mn} \left(\frac{k_{r\beta} \rho_\beta}{\mu_\beta} \right)_{mn} \left(X_\beta^{(k)} \right)_{mn} \left[\frac{P_{\beta,m} - P_{\beta,n}}{d_{mn}} - \rho_{\beta,mn} g \cos \theta \right] - \delta_{\beta,g} D_{va,mn} \rho_{\chi,mn} \frac{X_{\beta,m}^{(k)} - X_{\beta,n}^{(k)}}{d_{mn}}$$

236 (11)

237 The accuracy of the solution depends on the way interface parameters are expressed in function of average
 238 values on computing grid spatial elements. A general prerequisite is having an appropriate element subdivision
 239 in order to obtain equilibrium thermodynamic conditions in every cell and for every temporal step. For regular
 240 grids the discretized system would be identical to one obtained with a conventional finite difference discretized
 241 system. The entire fluid dynamic model implemented in Tough2RdS is based on the solution of a system of
 242 equations in primary variables, with coefficients dependent on secondary associated variables. The set of
 243 variables can be defined time after time depending on the typology of the problem or depending on fluid nature
 244 and composition. Issues related to fluid dynamic and physical characteristics and related to the number and
 245 type of components (water, CO₂, air, brine, NaCl, T, P, heat, etc.) are managed by a unique module, defined
 246 as equation-of-state (EOS) module. Once we have selected the appropriate EOS module, Tough2RdS code
 247 is able to independently manage the calculations, regardless of the type of fluid system located in the
 248 geological formation, including heat transfer process. This potential variability of parameters is fundamental to
 249 allow the application of the code to extremely diversified research field, such as CO₂ storage, high or low
 250 enthalpy geothermal energy, air storage etc. With reference to the investigated case study, EOS7 module
 251 considers as components pure water, brine and air as components of the fluid system, assuming pressure,
 252 air/brine fraction, temperature and gas phase saturation as primary variables. This module has been chosen

253 because it can treat different fluid mixtures and it allows to operate both in isothermal and non-isothermal
254 conditions, accounting heat balance equation with the possibility of activating different molecular diffusion
255 models. These options make this state module dedicated to the study of geothermal issues.

256 **5. Model comparison with original TOUGH2 code and FLS (Finite Line-Source) model**

257 The application of GeoSIAM, initially related to CCS, has been extended to many subsurface applications
258 including geothermal simulations. This led to a serious modification of the original TOUGH2 code [36] in order
259 to speed up computational times and to optimize it for geothermal case studies related to high, medium and
260 low enthalpy. Therefore it was necessary to perform a series of functional tests aimed at validating the new
261 computational code in light of the numerous modifications made to the software, both from a computational
262 and physical standpoint. The executed functional tests are:

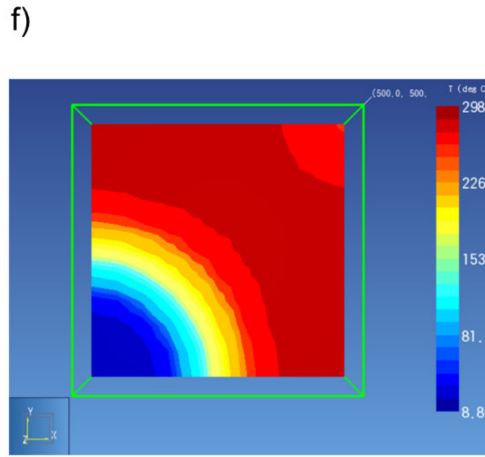
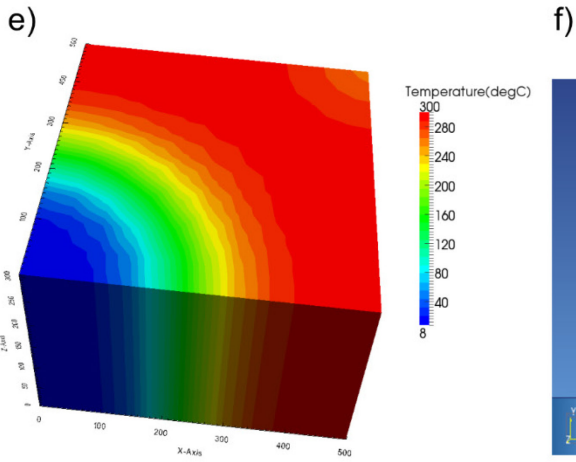
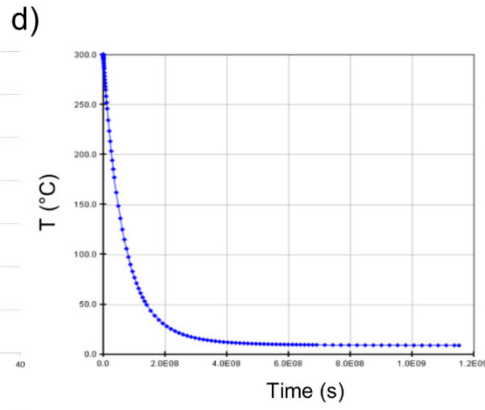
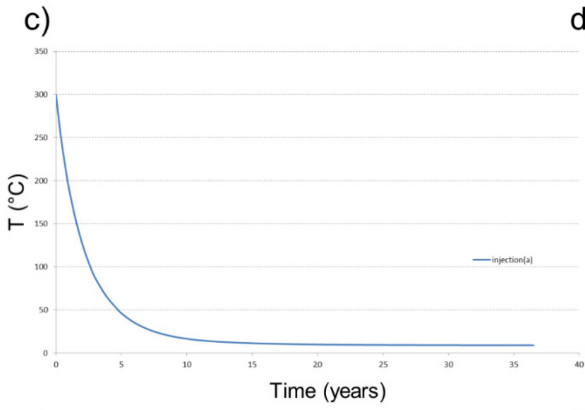
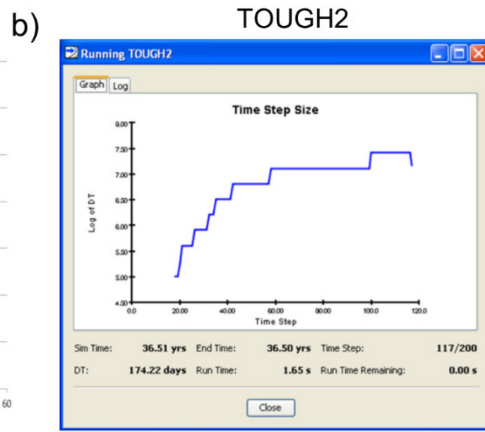
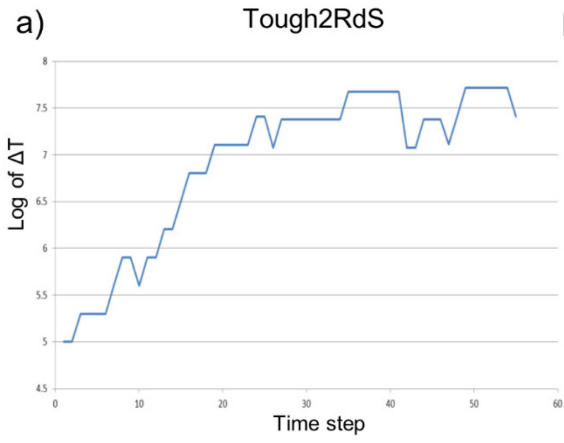
- 263 • tests supplied with original version of TOUGH2 [36];
- 264 • tests in literature available at [37].

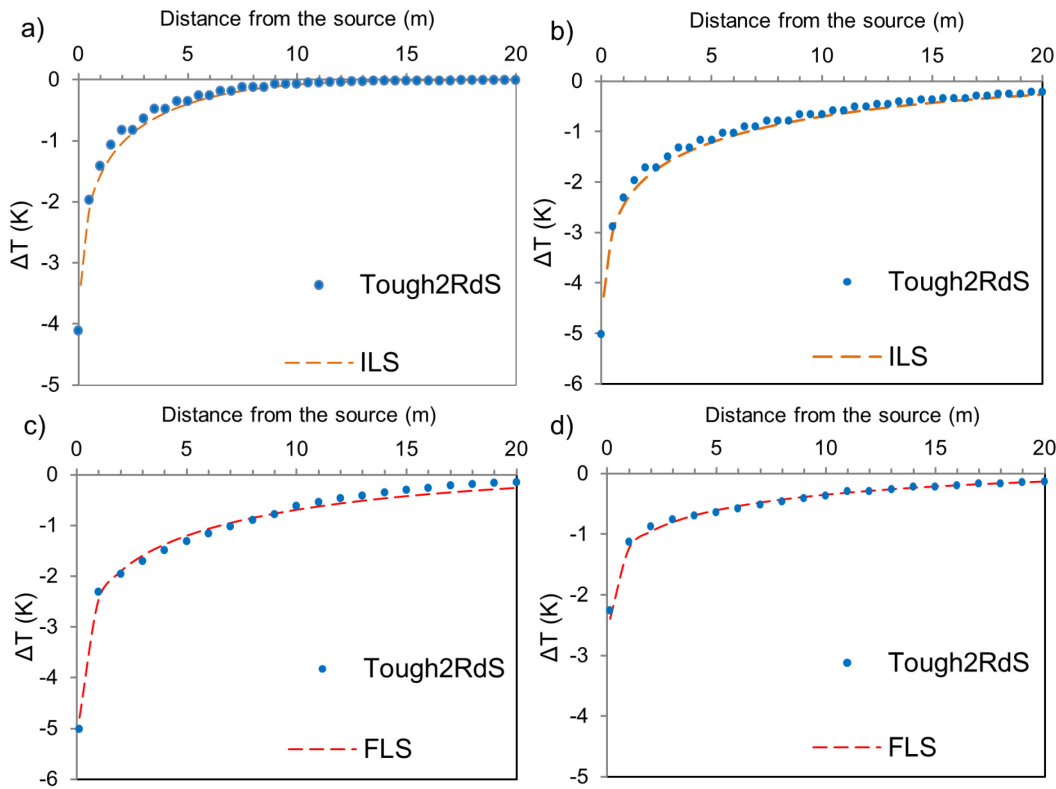
265 All verification tests were carried out and reported into the document [38]. In this paper one of the executed
266 simulation tests, called “Five-spot Geothermal Production and Injection” and described in [37] is reported. The
267 case study was analyzed with both Tough2RdS and PETRASIM [39], an interface for the original computational
268 code TOUGH2 and output results have been compared. Fig. 5a and Fig. 5b show the comparison between
269 data related to convergence parameters: number and length of temporal steps are reported and it is evident
270 that Tough2RdS uses wider temporal steps but the number of steps is halved (55 vs. 117). This is caused by
271 both a greater precision of the calculator and the improvements inserted in the management criteria of the
272 solver. Another comparison involved injection cell temperature during transient simulation (Fig. 5c and Fig. 5d).
273 From the comparison it is possible to observe a strong agreement between temperature trends. The final
274 comparison involved 3D temperature distributions within the domain, showing a perfect agreement (Fig. 5e
275 and Fig. 5f).

276 A second type of validation was carried out comparing Tough2RdS with the well-known infinite line-source
277 (ILS) and finite line-source (FLS) models commonly used in literature to analytically simulate thermal exchange
278 between geothermal probes and subsurface [15] [40]. A computing grid of 100 x 100 x 100 m (length x width x
279 depth) was created for the comparison with the ILS model while a computing grid of 100 x 100 x 125 (length x
280 width x depth) was created for the comparison with the FLS model. The undisturbed ground temperature was
281 set to 288 K in both scenarios and probe length was set to 100 m while the average yearly power withdrawn
282 from the ground was set to 9 W/m for a simulation period of 10 years. Ground thermal properties were set as

283 reported in Table 3. The comparison between ILS model and Tough2RdS solutions was carried out after
284 simulation times of 1 year (Fig. 6a) and 10 years (Fig. 6b) while the comparison between the FLS model and
285 Tough2RdS model solutions was assessed at a depth of 50 m (Fig. 6c) and 100 m (Fig. 6d). Results show a
286 maximum difference of 0.22 K between ILS and Tough2RdS solutions while the maximum difference between
287 FLS model and Tough2RdS solution is quantified in 0.14 K.

288 Due to these numerical verifications, Tough2RdS was considered as an effective tool for undertaking both high
289 and low enthalpy geothermal simulations. TOUGH2 was previously used by some authors to model high
290 enthalpy geothermal reservoirs [41] [42] [43]. In this paper the application of the modified computational code
291 Tough2RdS has been tested for low enthalpy geothermal energy.





293

294

295

296

6. Numerical model limitations and assumptions

297

Components that affect heat exchange in medium to large GSHP systems are too many to consider, even for the most sophisticated 3D model. In order to simplify the conceptual model, in this paper some assumptions were made:

299

300

- ❖ Borehole is assumed as a cylindrical heat source/sink, no simulations of fluid circulation in inlet/outlet pipes;

301

302

- ❖ No groundwater flow;

303

- ❖ Upper 10 meters of subsurface are affected by different meteorological conditions during the year. For this reason a climatic model that could provide superficial boundary conditions would be needed. In this paper the effects of GSHP on the first 10 m of subsurface were considered as negligible for the analyzed vertical system, therefore they were constrained to constant temperature. Climatic variables such as meteorological models for the first 10 meters of subsurface are currently under development;

304

305

306

307

308

- ❖ Heat probe system runs 24 h continually each day for the simulation period and there are no daily switch off. It is believed that thermal response of the subsurface over long time-scales (months or years) is mainly affected by overall heat extraction rather than the specific modes of heat exchange that affect small time-scales (minutes or hours).

309

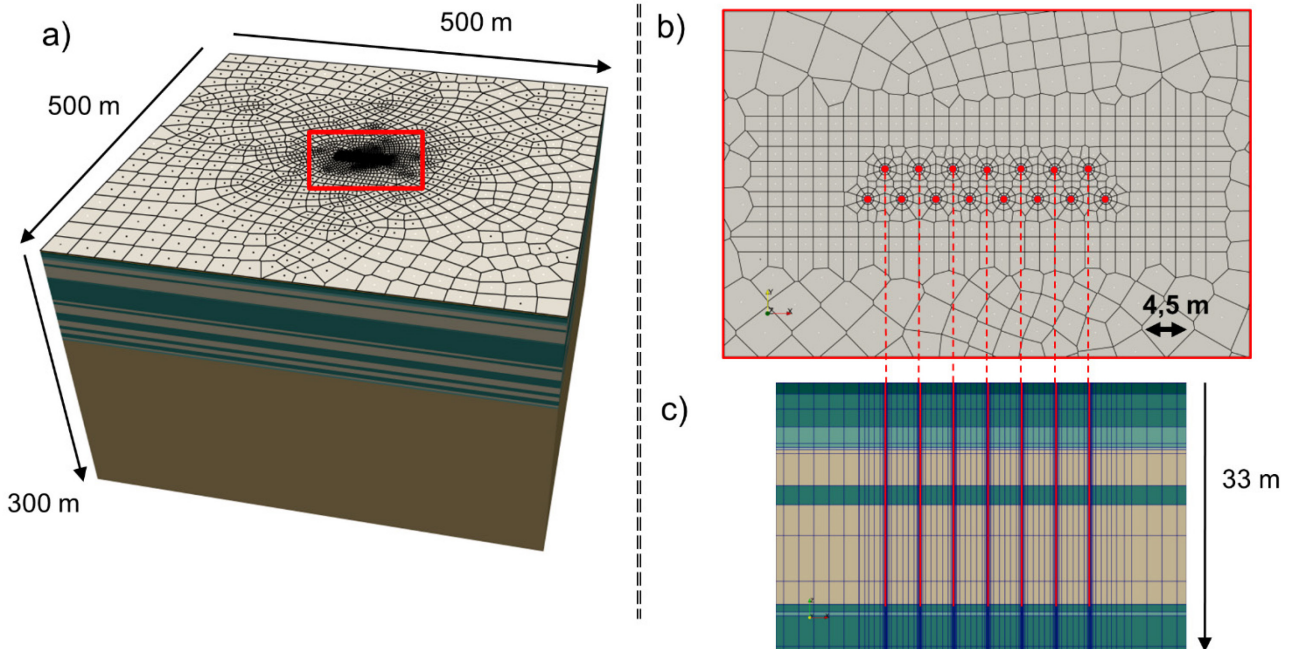
310

311

312

313 7. Numerical model

314



315

316 Performance and thermal imbalance issues highlighted in the previous chapters along with efficiency studies
317 of GSHP systems reported in literature [44] [45] suggest that the key factors to investigate in this particular
318 case study should basically be related to the effects of ground thermal properties and mutual probe distance.
319 From this starting premise, different scenarios have been developed and have been evaluated with the
320 previously described GeoSIAM modeling suite. A 3D Integrated Finite Difference model was created with a
321 size of 500 x 500 x 300 m (length x width x depth) and the probe field was inserted at the center of the domain
322 in order to have a “far-field” (Fig. 7a and Fig. 7b) that could minimize the effects of horizontal and vertical
323 thermal boundary conditions. The model is composed of 20 layers as reported in Fig. 2 with approximately
324 80000 prismatic elements created. The simulation consists of a 1240 days period with a heating period of 182
325 days from October to March (as described in Table 2) alternated with 183 days of system stand-by (from April
326 to September). The overall heat extracted from the ground in an annual operation is quantified in 4.385E+11
327 J. The length of the simulation period allows to investigate both the annual behavior of the system as well as
328 the short-period behavior in ΔT trends. ΔT is the difference between the initial temperature computed at a
329 certain depth and the computed temperature at *i-th* time step. Longer simulation periods were not taken into
330 account because of the large simulation area and the consequent long computation times needed. The
331 undisturbed ground temperature was set to 293 K and an average geothermal gradient of 3 K every 100 meters

332 of depth was introduced as a lower boundary condition. Spatial analyses were initially performed considering
333 370 days operation in order to observe the annual system behavior and the cones of temperature decrease of
334 the single probe related to the overall interference phenomena. This could have not been observed after 365
335 days because the system was off.

336 *7.1 Ground heterogeneity*

337 Studies in literature reported that the ignoring of ground layers has little effect on GSHP modeling [29]. The
338 paper tries to investigate this particular assumption for this case study by creating two simulation scenarios:
339 one composed of the real ground and one composed of an isotropic, homogeneous ground. The comparison
340 of horizontal, vertical and 3D temperature distributions were performed for two distinct types of subsurface
341 settings :

- 342 a) Real ground: interpretation of local stratigraphy constituted of gravel and clay interspersed with sandy
343 lenses that stand above a sandstone substrate, with realistic physical and thermal properties as
344 reported in (Fig. 2). Dry and wet λ terms are related to the interpolation formula for heat conductivity
345 as a function of liquid saturation (S_1) used by TOUGH2. The use of dry λ values in geothermal modeling
346 is a precautionary measure, while the use of the wet record is recommended once determined the
347 presence of groundwater [46], as observed in this case.
- 348 b) Homogeneous ground: hypothetical presence of an homogeneous media as commonly used in
349 literature, characterized by isotropic physical and thermal properties. Thermal properties of the
350 homogeneous ground were determined averaging those of layers composing the heterogeneous
351 media described in Fig. 2. The resulting homogeneous ground is assumed to have a reference λ of
352 1,83 W/m K and in Table 3 the main parameters used for the homogeneous scenario are reported.

354 *7.2 Probe distance*

355 In order to understand the magnitude of the observed thermal interference, two mutual distances were set:

- 356 - Probe distance of 4.5 m as in the real case study GSHP layout that was implemented in MethodRdS
357 as shown in Fig. 7b;
- 358 - Probe distance of 7 m, that is an optimal value estimated following ASHRAE instructions [47] for this
359 probe field layout in order to avoid thermal interference among probes.

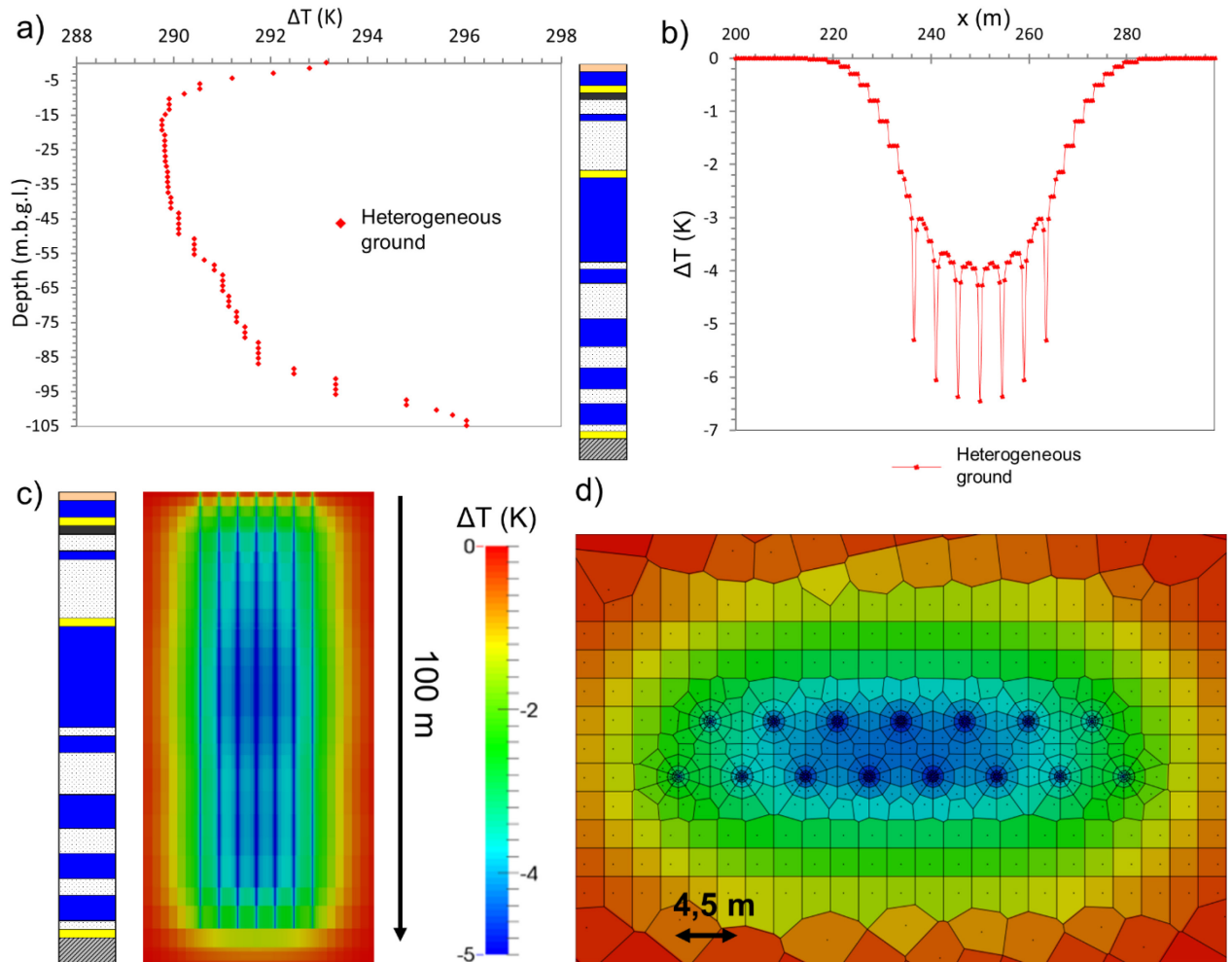
360 The particular layout of the probe field was maintained unchanged, with 7 probes in the northern row and 8 in
361 the southern one.

362 **8. Results and discussion**

363
364

8.1 One seasonal operation (winter and summer)

8.1.1 Real case study analysis

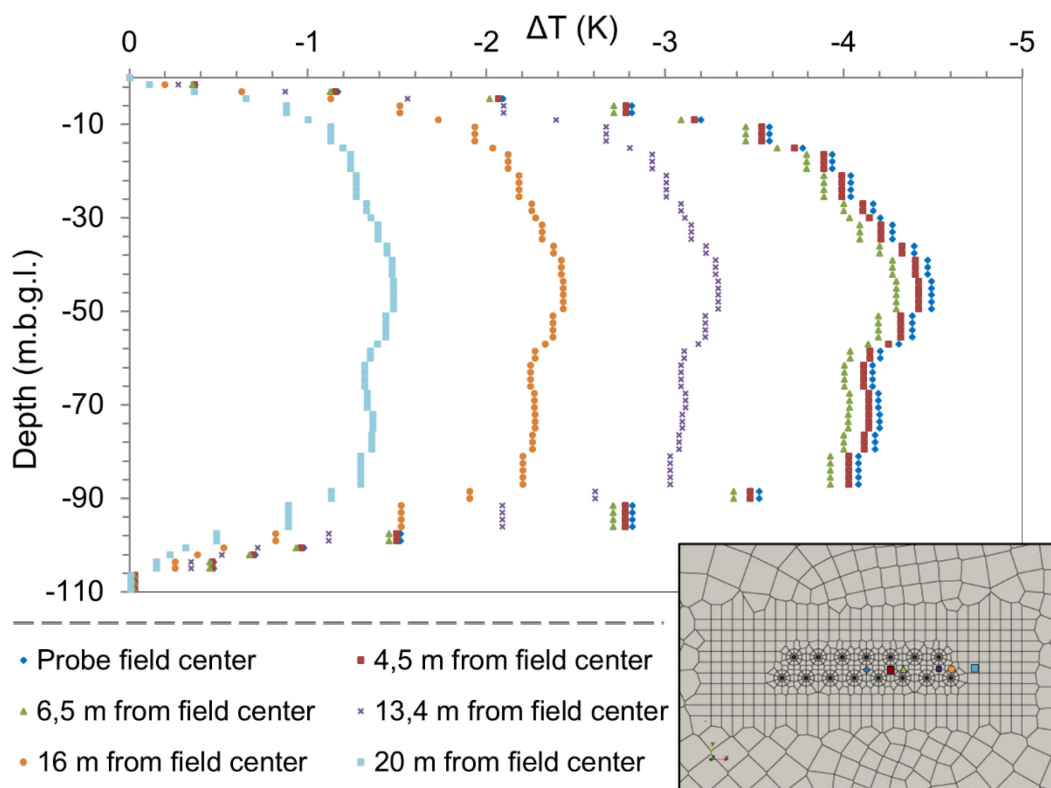


365

366 Fig. 8a shows vertical temperature profile for the real case study after 370 days from system power on in a
367 point located at the center of the probe field. The monitoring point at the center of the probe field was chosen
368 because it is affected by maximum probe interaction and can be used as an indicator for thermal imbalance
369 issues. Greater temperature variations are observed at a depth equal to $L/2$. This trend is due to the presence
370 of a 25 meters thick layer of clay with poor thermal properties. Local ground temperature is affected by greater
371 variations in clayey layer because they do not allow a proper heat diffusion, even in presence of groundwater.
372 In Fig. 8b, a horizontal profile of ΔT along the northern row of probes at a depth of 25 meters (gravels) is
373 reported. It is clearly visible the overall probe interference phenomena compared to the single probe “cone of
374 depression”. Each probe has a spatial influence on the surrounding soil limited to a diameter of few meters.
375 The overall interaction between probes produces a synergic effect very similar to the “cone of depression”
376 observed in pumping water wells. The influence of the whole probe field extends over 60 meters along main
377 (x) direction and over 30 meters along secondary (y) direction. Fig 8c and 8d show 3D ΔT distributions

378 respectively for a vertical and a horizontal section at 50 m depth where it is possible to understand the
 379 amplitude and magnitude of temperature variations.

380 A numerical analysis was performed in order to understand the magnitude of the interference phenomena
 381 depending on the distance from the center of the borehole field, identified as the most thermally critical point.
 382 Fig. 9 shows the synergic effect produced by probes interaction. If we proceed along horizontal direction ΔT
 383 values improve by 4%, 142% and 300% respectively for distances of 4.5 m, 16 m and 30 m from the center of
 384 the probe field to the eastern edge. Temperature variations in the ground are similar going from the center of
 385 the probe field within a 6.5 meters distance. This means that the interference phenomenon derives from the
 386 synergic simultaneous effect of 7 probes (as seen in Fig. 8d) and this is an intrinsic consequence of the probe
 387 field layout. The ground temperatures in the central region of the probe layout are lower than the peripheral
 388 ones, because heat diffuses with difficulty towards the center of the layout due to the thermal barrier of adjacent
 389 probes. If we proceed from the center towards the edge of the probe field for 13.5 m the magnitude of the
 390 interference lowers because ground temperature is only affected by 5 probes. Going at a distance of 20 m
 391 from the center it is clearly seen that temperature distribution is only affected by the outermost probe. At a
 392 distance of 30 meters from center the influence of the probe field on the surrounding soil becomes negligible.



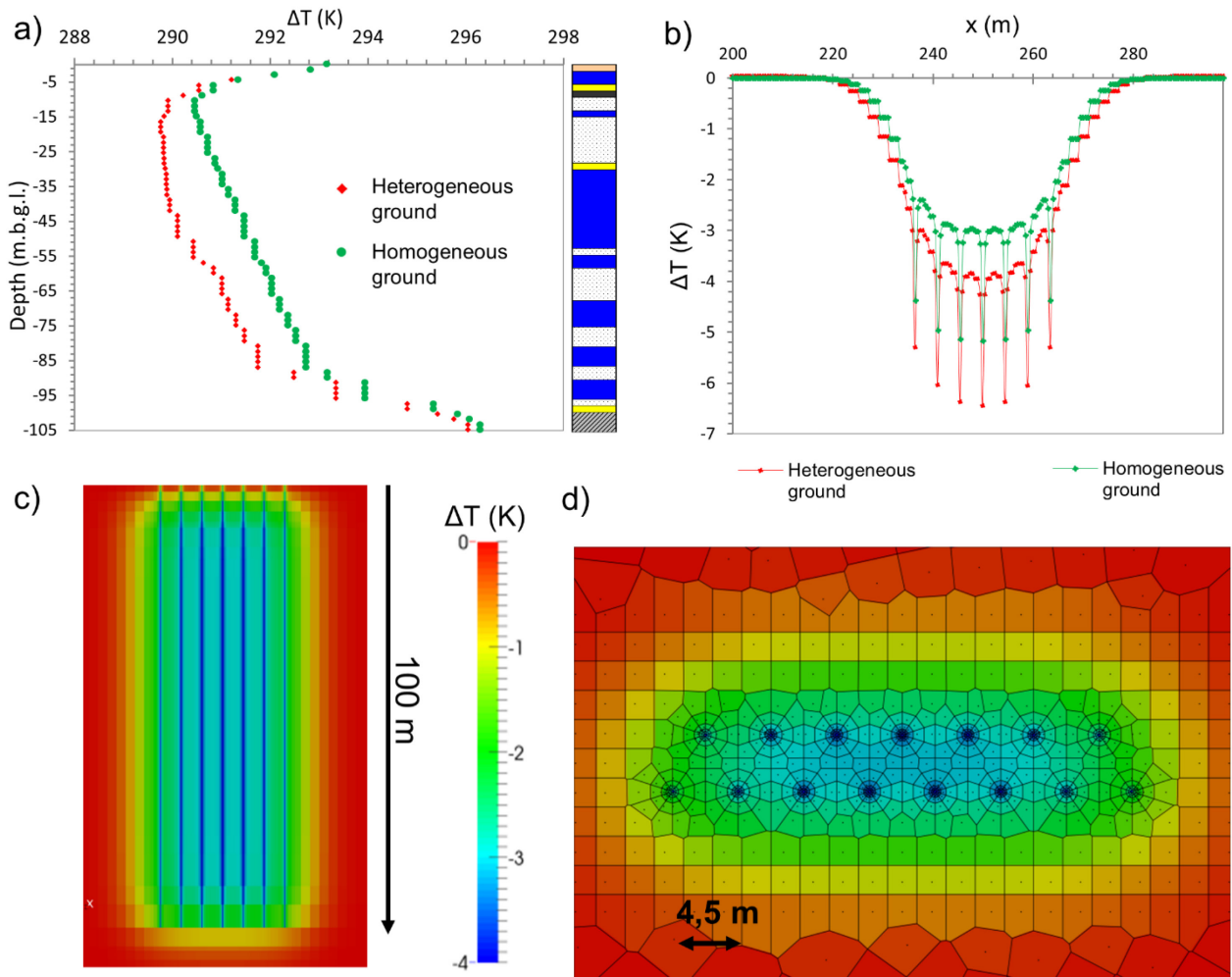
393

394 8.1.2 Homogeneous vs. heterogeneous ground

395

396 Higher thermal properties of the ground obtained by averaging those of the real case scenario allow to obtain
397 a greater thermal exchange. This leads to a reduction of thermal impact in the ground. Probe interference
398 effect is mitigated by greater heat exchange speed and higher heat storage of the medium.

399 From the comparison with real case it is possible to assert that heterogeneity considerably affects the behavior
400 of the probes (Fig. 10a) and vertical heat exchanges between layers are also more difficult than in a
401 homogeneous media. Under equal energy withdrawal and boundary conditions it is clearly seen how
402 temperature variations are greater in the heterogeneous scenario and temperature differences between two
403 types of stratigraphy are approximately quantified in 25%. The cone of temperature depression in the
404 heterogeneous scenario reaches higher values of ΔT (Fig. 10b). However, average thermal properties of the
405 local stratigraphy represented by homogeneous ground are still low if compared to those of subsurface
406 materials commonly used in literature and optimal for GSHP systems simulations (mainly rocks with $\lambda > 2$ W/m
407 K). A rocky setting is usually recommended for the installation of GSHP systems, because it has optimal
408 thermal properties such as great thermal conductivity, diffusivity and thermal capacity as well as a better
409 “resilience” against thermal overexploitations. This is one of the reason why European GSHP systems are
410 more easily found in regions characterized by the presence of rocky geological frameworks (Sweden,
411 Switzerland, Germany, France [3]) that ensure a fast heat transfer minimizing thermal imbalance issues.

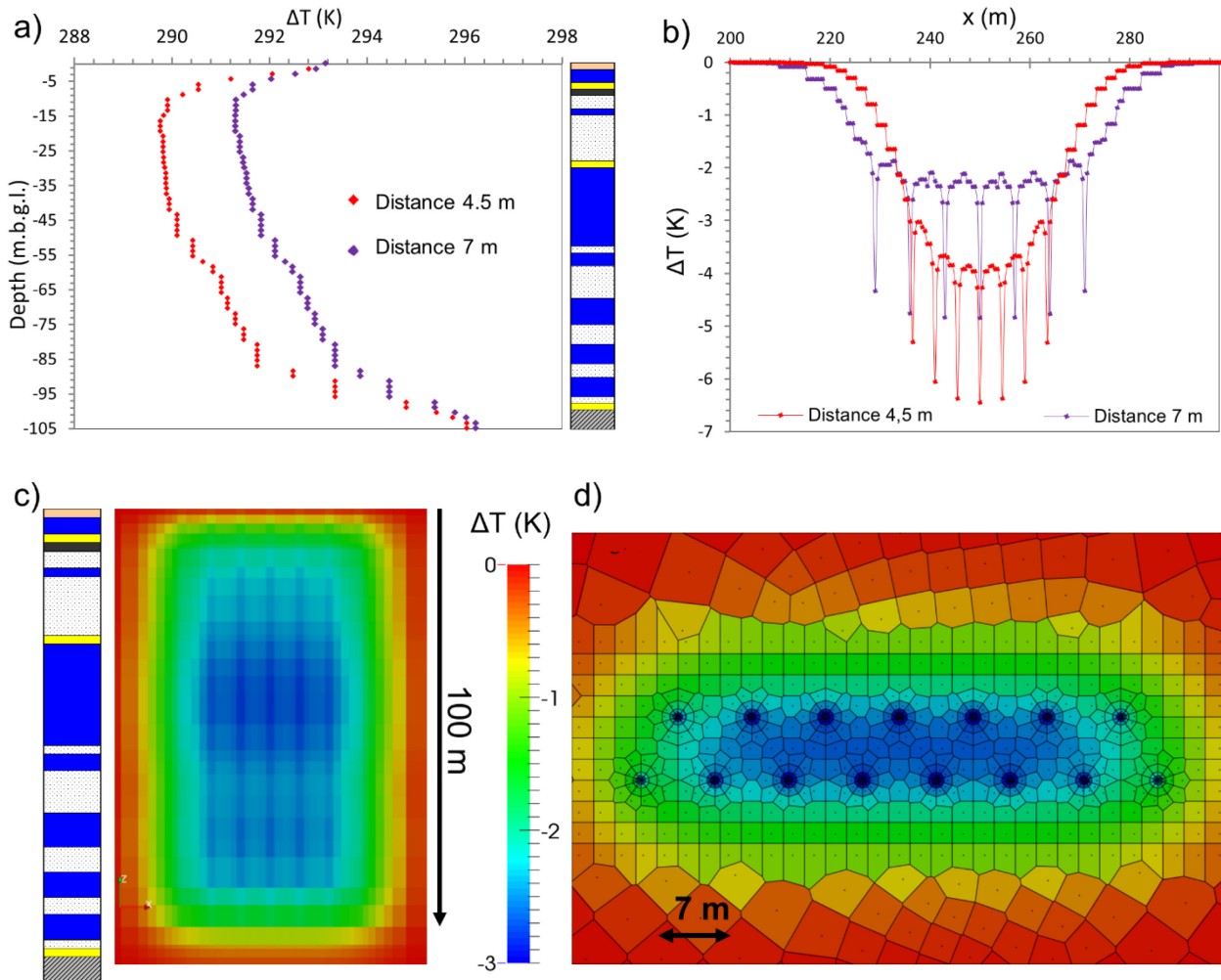


412

413 8.1.3 Effect of probe distance

414 The analysis of the real case (paragraph 8.1.1) took into account probe interaction phenomenon and the
 415 vertical temperature distribution at different distances from the probe field center. A new distance among
 416 probes was set to 7 meters (distance considered to be optimal for this case study) in order to understand the
 417 behavior of the temperature distribution for an increased distance. As probe distance increases from 4.5 meters
 418 to 7 meters, thermal imbalance issues decrease with maximum mitigation effects located at a depth of $L/2$
 419 where thick clayey layers are observed (Fig. 11c). Overall cone of thermal depression obviously extends for a
 420 larger distance from the field center but the simulated minimum temperature is far lower than the one simulated
 421 for the real case scenario. This implies that under equal energy extraction conditions and under equal thermal
 422 properties of the subsurface, thermal impact on the ground will be lower with a consequent improvement in
 423 system efficiency. Probe interaction phenomenon is still partially observed because it mainly depends on probe
 424 layout. The effect though is greatly mitigated because the synergic effect of cones of depression is way lower
 425 than in the real case as seen in Fig. 11b. GSH probe interference has many features in common with water
 426 wells interference: when two probes are close, the cones of depression may intersect and this intersection

427 increases the drawdown in both probes. Sometimes this additional drawdown may not affect probe yield but
 428 it could lead to higher pumping energetic costs because the heat must be withdrawn at a greater distance or
 429 depth. Usually the additional drawdown lowers the available amount of exploitable heat, causing system
 430 efficiency loss, as seen in this real case.



431

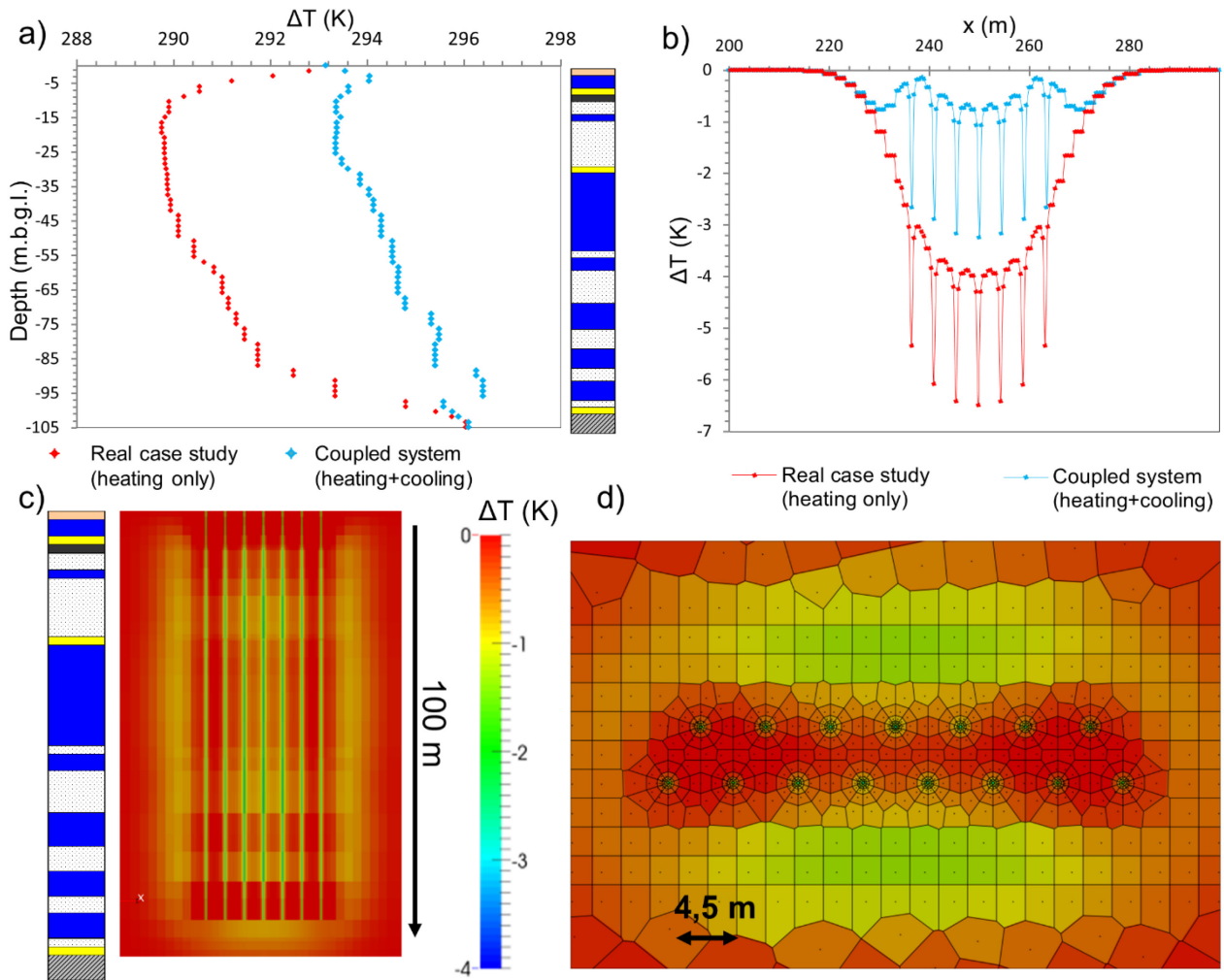
432 8.1.4 Additional cooling period scenario

433 Effects of ground heterogeneity and mutual probe distance clearly showed their influence on thermal field
 434 during an operating cycle in alluvial background. Another aspect that stands out is that the thermal energy
 435 requested for building conditioning is environmentally problematic compared to the natural thermal resilience
 436 properties of the analyzed alluvial subsurface and compared to probe distance. This leads to low temperature
 437 of the subsurface. Accordingly, potential mitigation effects that could be obtained through a hypothetical cooling
 438 period implemented in the operating cycles were investigated. However, it must be taken into account that the
 439 manufacturing technology of this particular system does not support coupling (irreversible system). The
 440 hypothesized cooling period lasts for 92 days, from the beginning of June to the end of August, with an
 441 estimated amount of heat injection of 65000 kW·h distributed as in Table 4. The new operating period is

442 constituted of 6 months of heating (as in previous cases, from October to March), 3 months of system inactivity
443 (April, May and September) and 3 months of cooling (June, July and August).

444 Fig. 12 a, b, c and d show that the simulated cooling period considerably mitigates thermal depletion within the
445 subsurface, even with a temperature increase of 1 K localized in the first 10 meters of depth. Gravelly layers
446 are less affected by both winter thermal depletion and summer heat injection due to their higher thermal
447 properties. This leads to a more stable temperature all over the year. At the other hand, clayey layers are more
448 affected by both thermal withdrawal and injection due to their low thermal properties. The cooling period reflects
449 on ΔT distribution with average mitigation effects of 70% than the real case simulation.

450 The hypothesized amount of injected heat still cannot completely balance thermal field because the amount
451 of heat requested for winter heating is far greater than for summer cooling and this is caused by the climatic
452 characteristics of the area, being an heating-dominated district. This behavior is seen in Fig. 12 b, c and d
453 where the distribution of ΔT is reported. Heat injection can balance the amount of heat extracted especially
454 within the volume occupied by the probe field. At the edge of the probe field low values of ΔT are still observed;
455 however the thermal field within the ground volume occupied by the probe field can be greatly reinstated after
456 1 year with relatively small amount of injected heat.



457

458

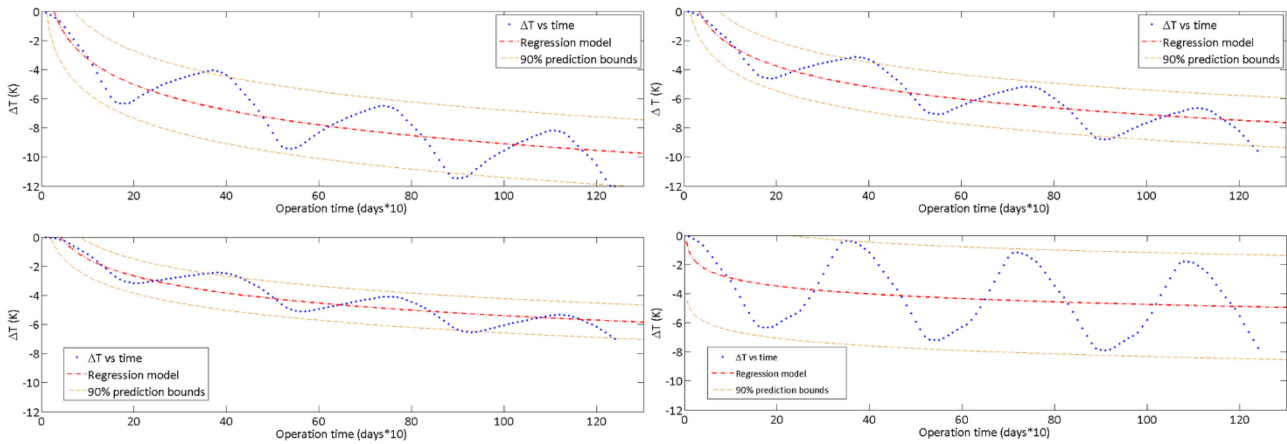
459 8.2 Short/medium term behavior

460 Evaluations on 1240 days simulations were carried out and the trends of ΔT in a point located at the center of
 461 the probe field with $z=-25$ m were analyzed. Every ΔT trend was then modeled using a regression formula that
 462 could describe the typical logarithmic trend of ground temperature in time for GSHP system caused by heat
 463 removal/injection and by natural reinstatement of the thermal field [48]. MATLAB software was used in order
 464 to perform data regression with the aim of estimating the time needed by the system to reach the average
 465 “perturbed stable temperature”. Ground temperature was considered stable when temperature variations
 466 within 10 days were lower than 0.01 K. This information is useful to understand when the system will reach
 467 stable performances and when an equilibrium between thermal energy demand and natural heat reinstatement
 468 capacities of the ground is reached. The regression was also used in order to hypothesize ΔT values that could
 469 be observed after 3, 5 and 10 years of system operation. Major statistics and prediction bounds of the
 470 regressions are also reported. Results in Fig. 13 and in Table 5 show that the real case scenario presents the
 471 lowest ΔT values and the temperature stabilizes after approximately 7 years of simulation. This is caused by

472 both probe distance and strong ground heterogeneity. Probe interference phenomenon creates a thermal
473 barrier which does not allow a complete reinstatement of ground temperature and this issue is amplified by
474 low thermal properties of the media that result in slow heat exchange. An homogeneous ground characterized
475 by better thermal properties contributes to shorten the time of ΔT stabilization by 20% and it also allows to
476 have an average temperature increase of 2.3 K. In the homogeneous scenario the negative and positive peaks
477 of temperature values tend to decrease in magnitude because the soil is less affected by heat
478 removal/reinstatement due to higher thermal properties. A ground with an higher thermal conductivity can
479 provide a greater amount of heat because can retrieve it from larger distances due to high heat propagation
480 speed. Thermal impact on the soil is lower than in the heterogeneous scenario and this affects stabilization
481 times because the system is able to reinstate the relatively perturbed thermal field after a shorter simulation
482 period. Improved distance scenario allows to obtain a 33% reduction in ΔT stabilization time as well as an
483 average temperature increase of 4.2 K. This is caused by a smaller probe interference phenomenon as the
484 cones of depression of adjacent probes have less influence on each other and the resulting ΔT is higher than
485 in a smaller distance scenario. The stabilization time is also smaller because ground temperatures are
486 subjected to a lower thermal stress and the system can reinstate a new "perturbed equilibrium" after a smaller
487 period. The coupled system shows the best performances in terms of stabilization times and perturbed ΔT with
488 achieved mitigations respectively of 68.5% and +5.5 K than real case because the heat removed is partially
489 replaced by the injected heat that joins the natural thermal reinstatement of the ground. The value of R^2
490 computed for the coupled scenario, though, is very low and performing a proper regression with this kind of
491 trend was difficult due to the great oscillation around an average value. However it is assumed that the ground
492 temperature trend for a coupled system could behave similarly as previously analyzed trends.

493 Results for the real case are in agreement with other simulations run using TRNSYS software [49] and reported
494 in RSE Report 11000459 [50].

495



496

497

498 **9. Discussion and conclusions**

499 In this paper a new fully 3D multi-proxy modeling analysis system was used in order to perform sustainability
 500 evaluation of a large scale GSHP system located in an heating-dominated district, characterized by a strongly
 501 heterogeneous subsurface. Influence of ground heterogeneity, probe distance and thermal imbalance issues
 502 were assessed. Short-term operation was simulated in order to understand the new ΔT values after system
 503 perturbation and to estimate medium-term stabilization times of ΔT using logarithmic data regression.

504 From overall model results described in this paper, it is possible to assert that alluvial deposits, such as those
 505 located in the Po Plain (due to its geomorphological characteristics) are problematic backgrounds for a medium
 506 to large scale GSHP system installation as the analyzed one because of their intrinsic low thermal properties,
 507 especially in heating dominated districts. Installing this GSHP system in a different region characterized, for
 508 example, by rocky geological context or by lower thermal energy demands would certainly reduce part of the
 509 thermal issues in the short period. Analyzed stratigraphies showed the presence of a rocky basement
 510 composed of sandstone with high thermal properties 10 meters under the probes lower limit. This media could
 511 be used to obtain a more efficient heat exchange with a possible mitigation of thermal imbalance problems
 512 and a reduction in probe number. The probe field could be deepened for other 20-30 meters in order to exploit
 513 the basement, however higher drilling costs must be taken into account.

514 Another critical variable is represented by mutual probe distance. A distance between adjoining probes of 4.5
 515 m leads to a strong over-exploitation of the ground thermal field for the given energy extraction rates, with a
 516 consequent loss of efficiency. The particular layout, designed for an adequate soil occupation, causes a strong
 517 interference phenomena between the 7 central probes. Thermal imbalance conditions in the ground will cause
 518 the GSHP system to operate at increasingly reduced capacities and may ultimately result in system failures
 519 due to the worsening of heat probe COP. As the temperature of the ground around boreholes becomes lower,

520 heat exchange becomes less efficient and the COP consequently decreases. A distance of 4.5 m between
521 probes seems to be too small for a sustainable performance of the system, given the requested energy
522 demands. This phenomenon is amplified by poor thermal properties of the ground, by the great amount of
523 requested energy and by operation times. Improving probe distance contributes to reduce stabilization times
524 by 33%, with a stabilized temperature of 4.3 K higher than in the real case study.

525 Data regressions report that the real case study scenario presents the longest time for temperature stabilization
526 and the lowest value of reached soil temperature. Results also show the importance of considering a layered
527 subsurface when dealing with strongly heterogeneous ground instead of an homogeneous model, as the
528 difference in ΔT for homogeneous/heterogeneous scenarios is approximately quantified in 25% and ΔT
529 stabilization times are reduced by 20%. Materials with poor thermal properties are affected by stronger thermal
530 imbalance issues and the assumption of homogeneous ground with average thermal properties seems to be
531 a little simplified in this case study. Homogeneous ground assumption arises from GRT results that give
532 averaged values of ground λ and are representative of a small area where the test is performed. For large
533 GSHP systems as the analyzed one where a strong heterogeneity is observed, single GRT cannot provide a
534 correct description of ground thermal characteristics.

535 Simulation of coupled system shows the strong mitigation effect of the additional cooling period on temperature
536 distribution even if the amount of heat injected for cooling purposes is hypothesized as half of the extracted
537 amount in the heating period. The coupled system produces the best mitigation effect even in presence of a
538 probe distance of 4.5 m, with a reduction in temperature stabilization times of 68.5% and average temperature
539 values of 5.5 K warmer than the real case study. Therefore, once established a strong probe interference
540 phenomenon amplified by poor thermal properties of the alluvial framework, it would be appropriate to build a
541 reversible system with an additional cooling period.

542 In this context the developed fully 3D-model seems to be profitably usable to properly consider geological,
543 energetic and engineering parameters of GSHP systems.

544

545 **Acknowledgments**

546 The study forms part of a RSE research project, called "Studies and assessments of rational use of electrical
547 energy" funded by the Italian Ministry of Economic Development as the D.M. 09/09/2012. I thank for his tireless
548 support Giordano Agate, an exemplary professional. I thank from the bottom of my heart Prof. Lucia De Biase
549 that gave me the opportunity to develop this thesis in the best possible way. Her advices and her faith in my
550 abilities allowed me to produce this scientific work and her premature departure left a massive void in my heart.

551
552
553
554
555
556
557
558
559
560
561
562
563
564
565
566
567
568
569
570
571
572
573
574
575
576
577
578
579
580
581
582
583
584
585
586
587
588
589
590
591
592
593
594
595
596
597
598
599
600
601
602
603
604
605
606
607

Software

The GeoSIAM modeling suite is publically available and can be requested to RSE Spa. For more information please contact Eng. Roberto Guandalini ^b: roberto.guandalini@rse-web.it

Figure captions

608 Figure 1. Territorial framework: the building in which the closed-loop GSHP system is installed is marked with
609 a violet triangle
610
611 Figure 2. Physical and thermal input parameters for the numerical model related to site subsurface (left) and
612 the created schematic stratigraphy (right)
613
614 Figure 3. COP trend during winter period
615
616 Figure 4. GeoSIAM GUI: Session Manager window
617
618 Figure 5. Comparison between Tough2RdS results and PETRASIM results for the simulated reference case
619 study
620
621 Figure 6. Numerical comparison between Tough2RdS and analytical models. a) comparison between ILS
622 and Tough2RdS after 1 year of simulation, b) after 10 years; c) comparison between FLS and Tough2RdS
623 after 10 years at $z = -50$ m, d) comparison between FLS and Tough2RdS after 10 years at $z = -100$ m
624
625 Figure 7. a) 3D model of the case study created with MethodRdS with a focus on b) probe field layout and on
626 c) an illustrative vertical section along the northern row of probes with the first 30 m of layered subsurface
627 highlighted
628
629 Figure 8. Real case scenario with heterogeneous ground. a) vertical profile of ΔT , b) horizontal profile of ΔT
630 at 25 m depth, c) vertical section of ΔT along the northern row of probes and d) horizontal section of ΔT field
631 at 50 m depth
632
633 Figure 9. Assessment of probe interference phenomenon. The graph shows the variation of ΔT vertical
634 profiles at different distances from probe field center while the probe field map at the bottom shows the
635 location of monitoring points.
636
637 Figure 10. Comparison between heterogeneous/homogeneous scenario after 370 days using a) vertical ΔT
638 profiles and b) horizontal ΔT profiles at $z = -25$ m. Figure c) represents vertical ΔT distribution along the
639 northern row of probes for homogeneous stratigraphy while figure d) represents horizontal section of ΔT field
640 at 50 m depth for homogeneous stratigraphy
641
642 Figure 11. Comparison between 4.5 m and 7 m probe distance after 370 days using a) vertical ΔT profiles
643 and b) horizontal ΔT profiles at $z = -25$ m. Figure c) represents vertical ΔT distribution along the northern row
644 of probes for 7 m scenario while figure d) represents horizontal section of ΔT field at 50 m depth for 7 m
645 scenario
646
647 Figure 12. Comparison between real case and coupled scenario using a) vertical ΔT profiles and b)
648 horizontal ΔT profiles at $z = -25$ m. Figure c) represents vertical ΔT distribution along the northern row of
649 probes for coupled system while figure d) represents horizontal section of ΔT field at 50 m depth for coupled
650 system
651
652 Figure 13. Simulated ΔT trends over a 1240 days period at 25 m depth for each scenario with data
653 regression logarithmic function and prediction bounds
654
655
656
657
658
659
660
661
662
663 Table 1. Summary of GSHP system characteristics and conditioned environment

Parameters related to heat probe and probes	
Heat probe model	TERRA MAX 70

IDM-Energiesysteme	
Nominal system power	67 kW
N° of geothermal probes	15
Probe type	1 U
Tube material	Pead 100
Grout thermal conductivity	1.38 W/m K
Probe length	100 m
Borehole diameter	150 mm
Borehole spacing	4.5 m
Building information	
N° of conditioned apartments	12
Single apartment area	80 m ²
Overall conditioned surface	960 m ²
Total conditioned volume	2592 m ³

664

665

666

667

668

Table 2. Average monthly values of monitored parameters (* Average over the working period; ** Total heat extracted from the ground)

Month	Mean air temperature (°C)	T inlet heat probe (°C)	T outlet heat probe (°C)	Heat extracted from the ground (kW·h)	Heat extracted from the ground (J)
October	10.7	8.5	6.4	8883	3.198E+10
November	9.3	7	4.9	18534	6.672E+10
December	4	3.6	1.6	23081	8.309E+10
January	1.4	2	0.1	32165	1.158E+11
February	3.7	1.5	-0.4	28654	1.032E+11
March	8.8	3.3	1.4	10500	3.780E+10
Overall working period	6.3*	4.3*	2.3*	121817	4.385E+11**

669

670

671

Table 3. Physical and thermal parameters for homogeneous ground

Parameter	Value
Porosity	20%
Density	1700 kg/m ³
Thermal conductivity	1.83 W/m K
Volumetric heat capacity	2.72 MJ/m ³
Specific Heat	1.6 KJ/kg K
Thermal diffusivity	7.6*10 ⁻⁷ m ² /s

672

673

674

Table 4. Hypothesized amounts of thermal energy injected in the ground for summer cooling

Month	Heat injected in the ground (kW·h)	Heat injected in the ground (J)
June	15000	5.400E+10
July	25000	9.000E+10

August	25000	9.000E+10
Entire summer period	65000	2.340E+11

675
676
677
678
679

Table 5. Estimate of medium-term ΔT values and stabilization times at the center of the probe field at 25 m depth after perturbation for every simulation scenario (* Stable $\Delta T = \Delta T$ variations within 10 days < 0.01 K)

Scenario	Average regression model	SSE	RMSE	R ²	Adj. R ²	Time to reach stable* ΔT (days)	Average ΔT After 3 Years (K)	Average ΔT After 5 Years (K)	Average ΔT After 10 Years (K)
Real case	$-2.526 \cdot \ln(x) + 2.536$	234.129	1.385	0.747	0.744	2540	-9.3 (± 2.6)	-10.6 (± 2.6)	-12.3 (± 2.6)
Homogeneous	$-2.0796 \cdot \ln(x) + 2.4743$	127.421	1.022	0.786	0.784	2090	-7.25 (± 2)	-8.35 (± 2)	-9.8 (± 2)
Distance 7 m	$-1.6927 \cdot \ln(x) + 2.3931$	61.031	0.707	0.835	0.834	1700	-5.65 (± 1.4)	-6.55 (± 1.4)	-7.7 (± 1.4)
Coupled	$-0.7862 \cdot \ln(x) - 1.1258$	559.223	2.141	0.107	0.099	800	-4.8 (± 4.2)	-5.2 (± 4.2)	-5.7 (± 4.2)

680
681
682
683
684
685
686
687
688
689
690
691
692
693
694
695
696
697
698
699
700
701
702
703
704
705
706
707
708
709
710
711
712
713
714
715
716
717
718

References

[1] W. Goetzler, R. Zogg, H. Lisel, J. Burgos, Ground-source heat probes: Overview of market status, barriers to adoption, and options for overcoming barriers, Navigant Consulting, Inc. Submitted to the US Department of Energy, Energy Efficiency and Renewable Energy, Geothermal Technologies Program, 10 (2009).

719
720 [2] J.W. Lund, D.H. Freeston, T.L. Boyd, Direct utilization of geothermal energy 2010 worldwide review,
721 Geothermics, 40 (2011) 159-180.
722
723 [3] P. Bayer, D. Saner, S. Bolay, L. Rybach, P. Blum, Greenhouse gas emission savings of ground source
724 heat probe systems in Europe: A review, Renewable and Sustainable Energy Reviews, 16 (2012) 1256-
725 1267.
726 [30]D.P.R. 26 agosto 1993, n. 412.
727
728 [4] I.B. Fridleifsson, R. Bertani, E. Huenges, J.W. Lund, A. Ragnarsson, L. Rybach, The possible role and
729 contribution of geothermal energy to the mitigation of climate change, IPCC scoping meeting on renewable
730 energy sources proceedings, Luebeck, Germany, Citeseer, 2008, pp. 59-80.
731
732 [5] T. Kurevija, D. Vulin, V. Krapec, Effect of borehole array geometry and thermal interferences on
733 geothermal heat probe system, Energy Conversion and Management, 60 (2012) 134-142.
734
735 [6] H. Cho, J.M. Choi, The quantitative evaluation of design parameter's effects on a ground source heat
736 probe system, Renewable Energy, 65 (2014) 2-6.
737
738 [7] F. Robert, L. Gosselin, New methodology to design ground coupled heat probe systems based on total
739 cost minimization, Applied Thermal Engineering, 62 (2014) 481-491.
740
741 [8] J. Spitler, C. Yavuzturk, S. Rees, In situ measurement of ground thermal properties, in: Proceedings of
742 terrastock, 2000, pp. 165-170.
743
744 [9] A.D. Chiasson, S.J. Rees, J.D. Spitler, A preliminary assessment of the effects of groundwater flow on
745 closed-loop ground source heat probe systems, ASHRAE Transactions 2000; Volume 106, Part 1, 929
746 pages, (2000).
747
748 [10] O. Zogou, A. Stamatelos, Effect of climatic conditions on the design optimization of heat probe systems
749 for space heating and cooling, Energy Conversion and Management, 39 (1998) 609-622.
750
751 [11] P. Healy, V. Ugursal, Performance and economic feasibility of ground source heat probes in cold climate,
752 International Journal of Energy Research, 21 (1997) 857-870.
753
754 [12] U. Desideri, N. Sorbi, L. Arcioni, D. Leonardi, Feasibility study and numerical simulation of a ground
755 source heat probe plant, applied to a residential building, Applied Thermal Engineering, 31 (2011) 3500-
756 3511.
757
758 [13] E.W. Heinonen, M.W. Wildin, A.N. Beall, R.E. Tapscott, Anti-Freeze Fluid Environmental and Health
759 Evaluation-An Update, Proceedings of the Second Stockton International Geothermal Conference, (1996) p.
760 1-11.
761
762 [14] H. Li, K. Nagano, Y. Lai, K. Shibata, H. Fujii, Evaluating the performance of a large borehole ground
763 source heat probe for greenhouses in northern Japan, Energy, 63 (2013) 387-399.
764
765 [15] P. Eskilson, Thermal Analysis of Heat Extraction Boreholes, Thesis, Department of Mathematical
766 Physics, Lund Institute of Technology, Lund, Sweden, 1987.
767
768 [16] S.P. Kavanaugh, K.D. Rafferty, Ground-source heat probes: design of geothermal systems for
769 commercial and institutional buildings, American Society of Heating, Refrigerating and Air-Conditioning
770 Engineers, 1997.
771
772 [17] H.Y. Zeng, N. R. Diao, Z. H. Fang, A finite line-source model for boreholes in geothermal heat
773 exchangers, Heat Transfer, Asian Research, 31 (2002) 558-567.
774
775 [18] L. Lamarche, B. Beauchamp, A new contribution to the finite line-source model for geothermal
776 boreholes, Energy and Buildings, 39 (2007) 188-198.
777
778 [19] J. Gao, X. Zhang, J. Liu, K. Li, J. Yang, Numerical and experimental assessment of thermal performance
779 of vertical energy piles: an application, Applied Energy, 85 (2008) 901-910.
780

781 [20] Y. Nam, R. Ooka, S. Hwang, Development of a numerical model to predict heat exchange rates for a
782 ground-source heat probe system, *Energy and Buildings*, 40 (2008) 2133-2140.
783

784 [21] P. Cui, H. Yang, Z. Fang, Numerical analysis and experimental validation of heat transfer in ground heat
785 exchangers in alternative operation modes, *Energy and Buildings*, 40 (2008) 1060-1066.
786

787 [22] J. Hecht-Méndez, M. De Paly, M. Beck, P. Bayer, Optimization of energy extraction for vertical closed-
788 loop geothermal systems considering groundwater flow, *Energy Conversion and Management*, 66 (2013) 1-
789 10.
790

791 [23] S.-K. Kim, G.-O. Bae, K.-K. Lee, Y. Song, Field-scale evaluation of the design of borehole heat
792 exchangers for the use of shallow geothermal energy, *Energy*, 35 (2010) 491-500.
793

794 [24] R. Perego, Studio dell'impatto di un gruppo di pompe di calore sul campo geotermico a medio
795 e lungo termine ed a scala di condominio e/o quartiere, M.Sc thesis in Environmental and Earth Sciences,
796 Academic year 2010-2011, University of Milano Bicocca, 107 pp. (unpublished)
797

798 [25] G. Ciampa, R. Costabile, F. Moia, R. Guandalini, S. Beretta, F. Cappelletti, S. Chiesa, Caratterizzazione
799 geologica del potenziale geoscambio e modellistica termica del Sottosuolo, RSE Report 11000671 (2011)
800 <http://www.rse-web.it/documenti/documento/314074> (in Italian).
801

802 [26] P. Canavese, E. Sesia, P. L. Rampa, Indagini e studi finalizzati alla predisposizione del Piano di Tutela
803 delle Acque - Elaborazioni dei dati qualitativi delle acque sotterranee, Parte generale - Rapporto Tecnico,
804 Regione Piemonte, ARPA Lombardia, 2003, pp. 47 (in Italian).
805

806 [27] F. Tinti, *Geotermia per la climatizzazione*, Dario Flaccovio editore, 2008 (in Italian).
807

808 [28] VDI 4640-1: VDI 4640 Blatt 1: Thermische Nutzung des Untergrundes: Grundlagen, Genehmigungen,
809 Umweltaspekte, 31 S. Verein Deutscher Ingenieure, Düsseldorf (2000)(in German).
810

811 [29] C. Lee, Effects of multiple ground layers on thermal response test analysis and ground-source heat
812 probe simulation, *Applied Energy*, 88 (2011) 4405-4410.
813

814 [30] Regolamento recante norme per la progettazione, l'installazione, l'esercizio e la manutenzione degli
815 impianti termici degli edifici ai fini del contenimento dei consumi di energia, in attuazione dell'art. 4, comma 4,
816 della L. 9 gennaio 1991, n. 10 (in Italian).
817

818 [31] L. Qiu, M. Yan, Research on Primary Energy Ratio of the Gas Engine-driven Heat Probe under Different
819 Run Mode, in: *Power and Energy Engineering Conference (APPEEC), 2010 Asia-Pacific, IEEE, 2010*, pp. 1-
820 4.
821

822 [32] Delibera EEN 3/08, Autorità Per L'energia Elettrica E Il Gas, Aggiornamento del fattore di conversione
823 dei kW·h in tonnellate equivalenti di petrolio connesso al meccanismo dei titoli di efficienza energetica, 2008
824 (in Italian).
825

826 [33] R. Guandalini, G. Agate, S. Beretta, F. Cappelletti, A. Amicarelli, F. Colucci, M. Valagussa, Fluid-dynamic
827 and geochemical numerical modeling of CO₂ storage reservoirs, RSE Report 12001257 (2011),
828 <http://www.rse-web.it/documenti/documento/314810> (in Italian).
829

830 [34] A. Henderson, J. Ahrens, C. Law, *The ParaView Guide*, Kitware Clifton Park, NY, 2004.
831

832 [35] G. Voronoi, Nouvelles applications des paramètres continus à la théorie des formes quadratiques.
833 Deuxième mémoire. Recherches sur les paralléloèdres primitifs, *Journal für die reine und angewandte*
834 *Mathematik*, 134 (1908) 90.
835

836 [36] K. Pruess, G. Moridis, C. Oldenburg, *TOUGH2 user's guide, version 2.0*, Lawrence Berkeley National
837 Laboratory Berkeley, 1999.
838

839 [37] <http://www.thunderheadeng.com/downloads/petrasim/4/examples/PetraSimExamples.pdf>
840

- 841 [38] R. Guandalini, G. Agate, Extension of fluid-dynamic and mechanical modeling of SIAM to small scale
842 studies for detailed analysis of extraction/injection processes, RSE Report 13000781 (2013), [www.rse-](http://www.rse-web.it/documenti/documento/315303)
843 [web.it/documenti/documento/315303](http://www.rse-web.it/documenti/documento/315303) (in Italian).
844
- 845 [39] ThunderHead Engineering – PETRASIM, <http://www.thunderheadeng.com/petrasim/>
846
- 847 [40] H.S. Carslaw, J.C. Jaeger, Conduction of heat in solids, Oxford: Clarendon Press, 1959, 2nd ed., 1
848 (1959).
849
- 850 [41] A. Battistelli, C. Calore, K. Pruess, The simulator TOUGH2/EWASG for modelling geothermal reservoirs
851 with brines and non-condensable gas, Geothermics, 26 (1997) 437-464.
852
- 853 [42] K. Pruess, Numerical simulation of multiphase tracer transport in fractured geothermal reservoirs,
854 Geothermics, 31 (2002) 475-499.
855
- 856 [43] A.E. Croucher, M.J. O'Sullivan, Application of the computer code TOUGH2 to the simulation of
857 supercritical conditions in geothermal systems, Geothermics, 37 (2008) 622-634.
858
- 859 [44] A. Casasso, R. Sethi, Efficiency of closed loop geothermal heat probes: A sensitivity analysis,
860 Renewable Energy, 62 (2014) 737-746.
861
- 862 [45] W. Yang, Y. Chen, M. Shi, J.D. Spitler, Numerical investigation on the underground thermal imbalance of
863 ground-coupled heat probe operated in cooling-dominated district, Applied Thermal Engineering, 58(1)
864 (2013) 626-637.
865
- 866 [46] E. Di Sipio, S. Chiesa, E. Destro, A. Galgaro, A. Giaretta, G. Gola, A. Manzella, Rock thermal
867 conductivity as key parameter for geothermal numerical models, Energy Procedia, 40 (2013) 87-94.
868
- 869 [47] A. Handbook, HVAC Applications (2007), American Society of Heating, Refrigerating, and Air
870 Conditioning Engineers, Inc. Atlanta, GA, (2007).
871
- 872 [48] S. Li, W. Yang, X. Zhang, Soil temperature distribution around a U-tube heat exchanger in a multi-
873 function ground source heat probe system, Applied Thermal Engineering, 29 (2009) 3679-3686.
874
- 875 [49] University of Wisconsin - M.S.E. Laboratory, S.A. Klein, TRNSYS, a transient system simulation
876 program, Solar Energy Laboratoary, University of Wisconsin--Madison, (1979).
877
- 878 [50] A. Capozza, F. Madonna, Geothermal heat pumps: modelling and experimental studies, RSE Report
879 11000459 (2010), <http://www.rse-web.it/documenti/documento/313956> (in Italian)
880